

CROSS-CORRELATION OF TENERIFE DATA WITH GALACTIC TEMPLATES — EVIDENCE FOR SPINNING DUST?

ANGÉLICA DE OLIVEIRA-COSTA^{1,2}, MAX TEGMARK^{1,3}, CARLOS M. GUTIERREZ⁴, ALED W. JONES⁵, R. D. DAVIES⁶, A. N. LASENBY⁵, R. REBOLO⁴ & R. A. WATSON^{6,4}

Draft version October 7, 2018

ABSTRACT

The recent discovery of dust-correlated diffuse microwave emission has prompted two rival explanations: free-free emission and spinning dust grains. We present new detections of this component at 10 and 15 GHz by the switched-beam Tenerife experiment. The data show a turnover in the spectrum and thereby supports the spinning dust hypothesis. We also present a significant detection of synchrotron radiation at 10 GHz, useful for normalizing foreground contamination of CMB experiments at high-galactic latitudes.

Subject headings: cosmic microwave background – diffuse radiation – radiation mechanisms: thermal and non-thermal – methods: data analysis

1. INTRODUCTION

Understanding the diffuse microwave emission from the Galaxy is crucial for doing cosmology with Cosmic Microwave Background (CMB) anisotropies. Although three components of Galactic emission have been firmly identified (synchrotron and free-free radiation, and thermal emission from dust particles), it is important to better quantify their frequency dependence and spatial distribution (see, *e.g.*, Kogut *et al.* 1996a; Tegmark *et al.* 1999 and references therein).

Cross-correlations of CMB data with far-IR maps have shown the existence of a microwave emission component whose spatial distribution is traced by these maps (Kogut *et al.* 1996b; Lim *et al.* 1996; de Oliveira-Costa *et al.* 1997; Leitch *et al.* 1997; de Oliveira-Costa *et al.* 1998, hereafter dOC98). Although this emission component has a spectral index suggestive of free-free emission (Kogut 1999), the correlations between H α and dust maps have been found to be marginal (McCullough 1997; Kogut 1997). The source of this correlated emission is therefore an open question. Recent work suggests that it originates from spinning dust grain emission (Draine and Lazarian 1998), which should have a spectral index of $-3.3 < \beta_{spin} < -4$ between 19 and 53 GHz. Since spinning dust grains have a predicted turndown in their emission at frequencies below 20 GHz, a cross-correlation analysis with lower frequency measurements may help to discriminate between free-free and spinning dust emission models.

The purpose of this letter is to evaluate the Galactic contribution in the Tenerife 10 and 15 GHz data sets by cross-correlating them with the DIRBE dust maps and with the Haslam and Reich and Reich synchrotron maps.

¹Institute for Advanced Study, Olden Lane, Princeton, NJ 08540; angelica@ias.edu

²Princeton University, Dept. of Physics, Princeton, NJ 08544

³Hubble Fellow

⁴Instituto de Astrofísica de Canarias, 38200 La Laguna, Tenerife, Spain

⁵Mullard Radio Astronomy Observatory, Cavendish Laboratory, Madingley Road, Cambridge, CB3 0HE, UK

⁶University of Manchester, Nuffield Radio Astronomy Laboratories, Jodrell Bank, Macclesfield, Cheshire, SK11 9DL, UK

Our analysis is based on the Tenerife measurements made up until the end of 1997 (Gutiérrez *et al.* 1999, hereafter G99). The Tenerife switched-beam experiment is a sky survey between $0^\circ \leq \text{RA} \leq 360^\circ$ and $30^\circ \leq \delta \leq 45^\circ$ (Figure 1 shows a sample strip at $\delta = 32^\circ$) carried out at an angular resolution of 5.1° FWHM with an instrument that uses a double-differencing technique. Data was taken at frequencies 10 and 15 GHz (we omit the 33 GHz data here due to lack of low latitude sky coverage), which are treated separately in order to gain additional frequency information on Galactic emission.

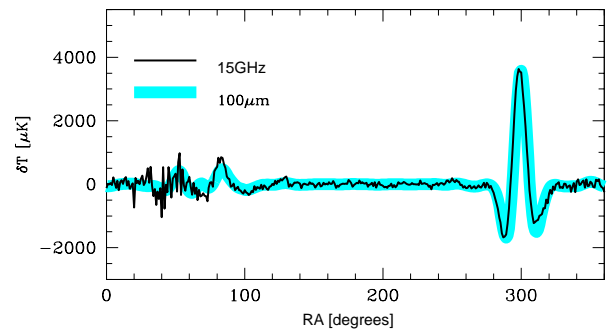


Fig. 1 — Scan of the Tenerife region $0^\circ < \text{RA} < 360^\circ$ for $\delta = 32^\circ$. The thin curve shows Tenerife 15 GHz data, while the thicker curve represents DIRBE $100\mu\text{m}$ convolved with the Tenerife triple-beam, rescaled for best fit. The spikes at $\text{RA} \sim 80^\circ$ and 300° correspond to the Galactic plane crossings.

2. METHOD

The Tenerife data consists of $N = 2880$ pixels at each frequency with double-differenced sky temperatures y_i and noise n_i . We assume that this data is a linear superposition of CMB fluctuations x_{CMB}^i and M Galactic components whose angular distributions are traced in part by external foreground templates. Writing these contributions as N -dimensional vectors, we obtain

$$\mathbf{y} = \mathbf{X}\mathbf{a} + \mathbf{x}_{CMB} + \mathbf{n}, \quad (1)$$

where \mathbf{X} is an $N \times M$ matrix whose rows contain the various foreground templates convolved with the Tenerife triple-beam (*i.e.*, \mathbf{X}_{ij} would be the i^{th} observation if the sky had looked like the j^{th} foreground template), and \mathbf{a} is a vector of size M that gives the levels at which these foreground templates are present in the Tenerife data.

We treat \mathbf{n} and \mathbf{x}_{CMB} as uncorrelated random vectors with zero mean, and the matrix \mathbf{X} as constant; thus the data covariance matrix is given by

$$\mathbf{C} \equiv \langle \mathbf{y}\mathbf{y}^T \rangle - \langle \mathbf{y} \rangle \langle \mathbf{y}^T \rangle = \langle \mathbf{x}_{CMB}\mathbf{x}_{CMB}^T \rangle + \langle \mathbf{n}\mathbf{n}^T \rangle. \quad (2)$$

The Tenerife noise covariance matrix $\langle \mathbf{n}\mathbf{n}^T \rangle$ is, to good approximation, diagonal (see Gutiérrez de la Cruz *et al.* 1995), while the CMB covariance matrix has the form

$$\langle \mathbf{x}_{CMB}\mathbf{x}_{CMB}^T \rangle_{ij} = \sum_{k=-1}^1 \sum_{l=-1}^1 w_k w_l c(\hat{\mathbf{r}}_{ik} \cdot \hat{\mathbf{r}}_{jl}), \quad (3)$$

where the vector $\mathbf{w} \equiv (-0.5, 1, -0.5)$ gives the weights of the three lobes in the Tenerife triple beam, $\hat{\mathbf{r}}_{i0}$ is the direction that the central lobe pointed to during the i^{th} observation, and $\hat{\mathbf{r}}_{i,\pm 1}$ is at the same declination but offset by $\pm 8.1^\circ$ on the sky. We take the CMB correlation function to be

$$c(\hat{\mathbf{r}}_{ik} \cdot \hat{\mathbf{r}}_{jl}) = c(\cos \theta) \equiv \sum_{\ell=2}^{\infty} B_\ell^2 C_\ell P_\ell(\cos \theta) \quad (4)$$

for a flat power spectrum $C_\ell \propto 1/\ell(\ell+1)$ normalized to a $Q_{flat} = (5C_2/4\pi)^{1/2} = 20\mu\text{K}$ (G99). Finally, we model the Tenerife beam as a Fisher function (Fisher *et al.* 1987)

$$B(\hat{\mathbf{r}} \cdot \hat{\mathbf{r}}') = \frac{\exp(\hat{\mathbf{r}} \cdot \hat{\mathbf{r}}'/\sigma^2)}{4\pi\sigma^2 \sinh(\sigma^{-2})} \quad (5)$$

with FWHM = $\sqrt{8 \ln 2} \sigma = 5.1^\circ$, which gives a window function $B_\ell \approx e^{-\sigma^2 \ell(\ell+1)/2}$. The Fisher function is locally Gaussian and integrates to unity over the unit sphere.

Since our goal is to measure \mathbf{a} , both \mathbf{n} and \mathbf{x}_{CMB} act as unwanted noise in equation (1). Minimizing $\chi^2 \equiv (\mathbf{y} - \mathbf{X}\mathbf{a})^T \mathbf{C}^{-1} (\mathbf{y} - \mathbf{X}\mathbf{a})$ yields the minimum-variance estimate of \mathbf{a} ,

$$\hat{\mathbf{a}} = [\mathbf{X}^T \mathbf{C}^{-1} \mathbf{X}]^{-1} \mathbf{X}^T \mathbf{C}^{-1} \mathbf{y}, \quad (6)$$

with covariance matrix

$$\boldsymbol{\Sigma} \equiv \langle \hat{\mathbf{a}}^2 \rangle - \langle \hat{\mathbf{a}} \rangle^2 = [\mathbf{X}^T \mathbf{C}^{-1} \mathbf{X}]^{-1}. \quad (7)$$

The error bars on individual correlations are therefore $\Delta \hat{a}_i = \boldsymbol{\Sigma}_{ii}^{1/2}$. This includes the effect of chance alignments between the CMB and the various template maps, since the CMB anisotropy term is incorporated in $\langle \mathbf{x}_{CMB}\mathbf{x}_{CMB}^T \rangle$.

3. DATA ANALYSIS & RESULTS

Due to the double-differencing technique, the Tenerife data are insensitive to the monopole ($\ell = 0$) and dipole ($\ell = 1$). Accordingly, when we convolve the template maps with the Tenerife triple beam function, we are removing the mean of the templates as well as large angular

scale structure. As a consequence, our results depend predominantly on the small scale intensity variations in the templates ($\ell \sim 10 - 30$) and are insensitive to the zero levels and gradients in the CMB and the template maps.

Table 1. – Correlations for 10 and 15 GHz data.

| b & ν | Template ^(a) | $\hat{\mathbf{a}} \pm \Delta \hat{\mathbf{a}}^{(b)}$ | $\frac{\hat{\mathbf{a}}}{\Delta \hat{\mathbf{a}}}$ | σ_{Gal} | ΔT [μK] ^(c) |
|----------------------------|-------------------------|--|--|----------------|---|
| $ b > 20^\circ$ 10 GHz | 100 μm | 49.8 \pm 11.2 | 4.5 | 0.8 | 38.1 \pm 8.5 |
| | Has | 29.5 \pm 5.9 | 5.0 | 1.0 | 30.8 \pm 6.1 |
| | R&R | 0.8 \pm 0.3 | 2.8 | 23.2 | 17.8 \pm 6.4 |
| 15 GHz | 100 μm | 71.8 \pm 4.5 | 5.9 | 0.7 | 52.8 \pm 3.3 |
| | Has | 0.8 \pm 3.4 | 0.2 | 1.1 | 0.8 \pm 3.7 |
| | R&R | 0.1 \pm 0.2 | 0.3 | 24.6 | 1.3 \pm 3.7 |
| $ b > 30^\circ$ 10 GHz | 100 μm | -8.3 \pm 31.9 | -0.3 | 0.2 | -1.9 \pm 7.2 |
| | Has | 35.8 \pm 8.8 | 4.1 | 0.9 | 31.1 \pm 7.6 |
| | R&R | 0.5 \pm 0.4 | 1.2 | 19.4 | 9.3 \pm 7.8 |
| 15 GHz | 100 μm | 94.9 \pm 15.3 | 6.2 | 0.3 | 24.9 \pm 4.0 |
| | Has | -8.3 \pm 5.0 | -1.7 | 0.9 | -7.3 \pm 4.4 |
| | R&R | -0.3 \pm 0.2 | -1.4 | 19.8 | -6.0 \pm 4.4 |
| $ b > 40^\circ$ 10 GHz | 100 μm | 84.6 \pm 54.8 | 1.5 | 0.2 | 14.6 \pm 9.6 |
| | Has | 24.1 \pm 11.4 | 2.1 | 0.8 | 19.4 \pm 9.1 |
| | R&R | 0.4 \pm 0.5 | 0.6 | 19.1 | 6.7 \pm 10.5 |
| 15 GHz | 100 μm | 72.4 \pm 33.3 | 2.2 | 0.2 | 12.3 \pm 5.7 |
| | Has | -10.8 \pm 6.3 | -1.7 | 0.8 | -8.7 \pm 5.1 |
| | R&R | -0.4 \pm 0.3 | -1.1 | 19.5 | -7.0 \pm 6.2 |

^(a) The DIRBE and Haslam correlations listed in this table correspond to joint 100 μm –Has fits, whereas the R&R numbers correspond to a joint 100 μm –R&R fit.

^(b) $\hat{\mathbf{a}}$ has units μK (MJy/sr)⁻¹ for the 100 μm template, $\mu\text{K/K}$ for the Has template and $\mu\text{K/mK}$ for the R&R template. We use antenna temperature throughout.

^(c) $\Delta T \equiv (\hat{\mathbf{a}} \pm \Delta \hat{\mathbf{a}}) \sigma_{Gal}$.

3.1. Correlations & Variances

We cross-correlate the Tenerife data with two different synchrotron templates: the 408 MHz survey (Haslam *et al.* 1981) and the 1420 MHz survey (Reich and Reich 1988), hereafter Has and R&R, respectively. To study dust and/or free-free emission, we cross-correlate the Tenerife data with three Diffuse Infrared Background Experiment (DIRBE) sky maps at wavelengths 100, 140 and 240 μm (Boggess *et al.* 1992). The extent of point source contamination in the Tenerife data is discussed and estimated in G99, and therefore will not be addressed in this *Letter*. In practice, we just remove the estimated point sources contribution before calculating the correlations. For definiteness, we use the DIRBE 100 μm channel when placing all limits below since it is the least noisy of the three DIRBE channels, and the Haslam map since it is the synchrotron template at lowest frequency.

Table 1 shows the coefficients $\hat{\mathbf{a}}$ and the corresponding fluctuations in antenna temperature in the Tenerife data ($\Delta T = \hat{\mathbf{a}} \sigma_{Gal}$, where σ_{Gal} is the standard deviation of the template map). The analysis is done for three different cuts: 20° , 30° and the *Tenerife cut* (which consists of data with $160^\circ < \text{RA} < 250^\circ$, corresponding to Galactic latitudes $|b| \gtrsim 40^\circ$). Note that the fits are done jointly for $M = 2$ templates. The DIRBE and Haslam correlations listed in Table 1 correspond to joint 100 μm –Has fits, whereas the R&R numbers correspond to a joint 100 μm –R&R fit.

Statistically significant ($> 2\sigma$) correlations are listed in boldface. The two synchrotron templates are found to be correlated with the 10 GHz data at low Galactic latitudes and this correlation persists with the Has template even at higher latitudes, while the 15 GHz data is not correlated with these templates even for a 20° cut. The $100\mu\text{m}$ and 10 GHz data are correlated only at lower Galactic latitudes (20° cut), while the correlation with the 15 GHz data persists to higher latitudes. The same analysis was carried out for the DIRBE $140\mu\text{m}$ and $240\mu\text{m}$ maps, giving very similar results.

3.2. Latitude Dependence

To investigate the dependence of the correlation on Galactic latitude, we sliced the maps into six regions of equal area, each corresponding to a range of latitude $|b|$. Figure 2 shows the results for the $100\mu\text{m}$ map. Note that $\hat{\alpha}$ from the $100\mu\text{m}$ –15 GHz correlation is similar in all latitude bands, suggesting that the particular ISM properties that are responsible for the correlation do not vary strongly with latitude.

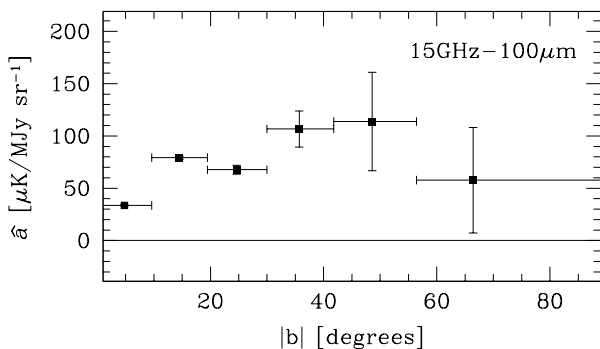


Fig. 2 — Dependence of $\hat{\alpha}$ on Galactic latitude for the $100\mu\text{m}$ –correlated emission at 15 GHz.

3.3. Spectral Index

Writing the frequency dependence as $\delta T \propto \nu^\beta$, we obtain interesting limits on the spectral index β . For synchrotron radiation, both the Has–10 GHz and the R&R–10 GHz correlations are consistent with $\beta \sim -3$ in all latitude slices. The most favored values between 408 MHz and 10 GHz values ($-3.2 \lesssim \beta \lesssim -3.4$) are slightly steeper than the canonical sub-GHz slope of $-2.7 \lesssim \beta \lesssim -2.9$ (Davies *et al.* 1998; Platania *et al.* 1998). Such a steepening of the spectrum at higher frequencies is consistent with a steepening of the spectrum of cosmic ray electrons at higher energies (Rybicki and Lightman 1979). For the emission component correlated with the $100\mu\text{m}$ map, the spectral index between 10 and 15 GHz is $0.80_{-0.77}^{+0.66}$ for $|b| > 20^\circ$, and the spectrum is also clearly rising at $|b| \gtrsim 30^\circ$ (see Table 1). Calibration uncertainties are below 5% in the Tenerife data at both 10 and 15 GHz, and therefore do not affect the conclusions that we will draw from this spectral behavior.

¹Systematic effects (such as striping) are present in the synchrotron radio maps and may be partially responsible for the uncorrelated part of their signal (Davies *et al.* 1998). In addition, detector noise in the template maps will of course also reduce their correlation with each other and with the Tenerife data, but is in our case negligible compared to the Tenerife noise.

3.4. Effect of Template Correlations

Equation (7) shows that we can interpret Σ^{-1} as measuring correlations between the various templates. Table 2 shows the dimensionless correlation coefficients $r \equiv \Sigma_{ij}^{-1} (\Sigma_{ii}^{-1} \Sigma_{jj}^{-1})^{-0.5}$, using the 10 GHz pixel weighting, and enables a number of conclusions to be drawn:

1. The three DIRBE maps are, as expected, highly correlated, *i.e.*, they trace the same warm dust emission;
2. The two synchrotron maps are less well correlated, with only $r^2 \sim 50\%$ of the variance in the Has map being traced by the R&R map at $|b| > 20^\circ$ cut, and even less at higher latitudes¹; and
3. All three DIRBE maps are seen to be almost uncorrelated with both radio maps, with the common variance r^2 being only a few percent. This means that Σ is almost diagonal, and that simply performing a separate correlation analysis for each component (with $N = 1$, as was done in *e.g.*, de Oliveira-Costa *et al.* 1997; dOC98) will give almost identical results to a joint ($N > 1$) analysis. We tested this, and indeed obtained results in good agreement with those presented in subsection 3.1).

Table 2. — Correlation between foreground templates^(a).

| | $100\mu\text{m}$ | $140\mu\text{m}$ | $240\mu\text{m}$ | Has | R&R |
|------------------|------------------|------------------|------------------|------|------|
| $100\mu\text{m}$ | 1 | 0.97 | 0.96 | 0.12 | 0.14 |
| $140\mu\text{m}$ | 0.91 | 1 | 0.98 | 0.08 | 0.11 |
| $240\mu\text{m}$ | 0.91 | 0.88 | 1 | 0.07 | 0.11 |
| Has | 0.11 | 0.12 | 0.11 | 1 | 0.71 |
| R&R | 0.15 | 0.11 | 0.17 | 0.53 | 1 |

^(a) The upper right triangle of the table uses a $|b| > 20^\circ$ cut and the lower left triangle a $|b| > 30^\circ$ cut.

3.5. Fake Skies

We tested our software by analyzing constrained realizations of the CMB and the Tenerife instrument noise. Cholesky decomposing the covariance matrix as $\mathbf{C} = \mathbf{L}\mathbf{L}^T$, we generated fake skies using $\mathbf{y} = \mathbf{L}\mathbf{z} + \mathbf{X}\mathbf{a}$, where \mathbf{z} is a vector of independent Gaussian random variables with $\langle \mathbf{z} \rangle = \mathbf{0}$ and $\langle \mathbf{z}\mathbf{z}^t \rangle = \mathbf{I}$ (the identity matrix), which gives $\langle \mathbf{y}\mathbf{y}^T \rangle - \langle \mathbf{y} \rangle \langle \mathbf{y} \rangle^t = \mathbf{L} \langle \mathbf{z}\mathbf{z}^T \rangle \mathbf{L}^T = \mathbf{L}\mathbf{L}^T = \mathbf{C}$. Analyzing 1000 such realizations, we recovered unbiased estimates $\hat{\mathbf{a}}$ with a variance in agreement with equation (7).

3.6. Sky Rotations

Systematic errors or unmodeled foregrounds may add non-Gaussian fluctuations to the the data set \mathbf{y} , making the true error bars larger than suggested by equation (7). To address this issue, we repeated the fit done in equation (6) after replacing the template map with a set of “control” patches selected from different portions in the sky. We repeated the analysis with $24 \times 2 \times 2 = 96$ transformed maps, rotated around the Galactic axis by multiples of 15° and/or flipped vertically and/or horizontally. The correct Haslam template has the highest of all

96 correlations with the 10 GHz data. Even for a $|b| \gtrsim 40^\circ$ cut, 95 of the 96 patches (or 99% of them) are less correlated with the the 10 GHz data than the correct $100\mu\text{m}$ patch. The same test was carried out for other Galactic cuts and the 15 GHz data, giving similar results. These results show that our correlations are not due to systematic errors or chance alignments between the CMB and the various template maps. We also applied the rotation test to the foreground template correlations in Table 2. Although as mentioned above, the dust-synchrotron correlations are tiny ($r \ll 1$) and negligible for our purposes, they are still statistically significant; for a 40° Galactic cut, the correct synchrotron template (Has or R&R) has the highest of all 96 correlations with the DIRBE map.

4. CONCLUSIONS

We have detected high-latitude galactic foreground signals in the Tenerife data at high ($\gtrsim 5\sigma$) statistical significance, summarized in Figure 3. The synchrotron signal is consistent with previous upper limits (Kogut *et al.* 1996b) and detections (dOC98), and provides a useful normalization for modeling microwave foregrounds. We also verify that the 15 GHz *Tenerife-cut* data is useful for CMB cosmology; although the DIRBE-correlated component is statistically significant, it is much smaller in amplitude than the primary cosmological signal.

Our results indicate that the DIRBE-correlated signal may turn out to be the dominant foreground seen by the the MAP satellite. What is its physical origin? A “smoking gun” indication of spinning dust grains would be a turnover in the spectrum, since all Draine and Lazarian models show such a feature whereas the antenna temperature of free-free emission continues to rise with $\beta \sim -2.1$ towards lower frequencies. Figure 3 combines our present results with previous measurements. The lower panel shows that the synchrotron spectrum is well fit by a power law ν^β with $\beta \sim -3$ (cyan line). In the upper panel, the dashed curve shows the spectrum for a best fit linear combination of vibrational (green) and rotational (yellow) dust emission. The vibrational spectrum assumes a 20K dust temperature and an emissivity of 2. The rotational spectrum is the warm interstellar medium model of Draine and Lazarian (1998) from www.astro.princeton.edu/~draine/. A joint three-parameter fit, including free-free emission with spectrum $\nu^{-2.15}$ as a third component (magenta), prefers negligible amounts of free-free above 10 GHz. On purely physical grounds, free-free emission must of course be present at some level. However, if the 10 GHz Tenerife correlation were entirely due to free-free emission, this component would explain only about 10% of the variance observed at 15 GHz and a percent of the variance in the Saskatoon data. The interpretation of such fits that directly compare data points from different experi-

ments is complicated by conversions between different angular scales (dOC98). However, a direct comparison between the 10 and 15 GHz Tenerife points from this work is straightforward, since the angular resolution and window functions are the same, and gives a spectral index of $\beta = 0.80_{-0.66}^{+0.77}$. This is clearly inconsistent with free-free emission, and provides evidence that the main culprit is indeed spinning dust.

The authors wish to thank Bruce Draine, Lyman Page, David Spergel and David Wilkinson for helpful comments. Support for this work was provided by NASA through grants NAG5-6034 and Hubble Fellowship HF-01084.01-96A (from STScI, operated by AURA, Inc. under NASA contract NAS5-26555), and NSF grant PHY-9600015. AWJ acknowledges King’s College, Cambridge, for support in the form of a Research Fellowship.

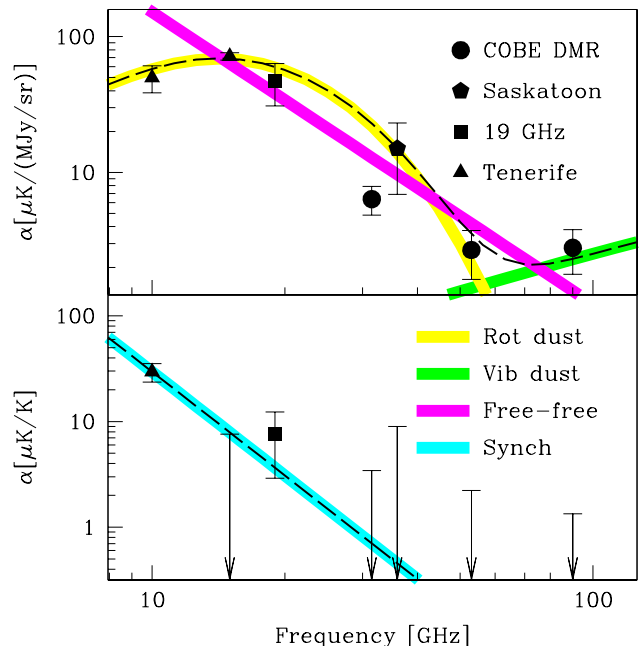


Fig. 3 — Frequency dependence of DIRBE-correlated emission (top) and Haslam-correlated emission (bottom). The DIRBE-correlated emission is seen to be approximately fit by a combination of spinning and vibrating dust (dashed curve), whereas free-free emission alone (falling straight line) cannot explain the drop from 15 to 10 GHz. The slope of the Haslam-correlated emission is seen to be weakly constrained, fitting e.g. a single $\beta = -3.26$ power law down to 408 MHz (where $\alpha = 10^6 \mu\text{K}/\text{K} = 1$ by definition). Tenerife data is from Table 1 for a 20° cut. Upper limits are $2\text{-}\sigma$. Note that the error bars on the 15 GHz point (top) are too small to be visible.

REFERENCES

- Bogges, N.W., *et al.* 1992, ApJ, 397, 420
 Davies R.D., Watson, R.A., and Gutierrez, C.M. 1998, MNRAS, 278, 925
 de Oliveira-Costa, A., *et al.* 1997, ApJ, 482, L17
 de Oliveira-Costa, A., *et al.* 1998, ApJ, 509, L9 (dOC98)
 Draine, B.T., and Lazarian, A. 1998, ApJ, 494, L19
 Fisher, N.I., Lewis, T. and Embleton, B.J.J. 1987, Statistical Analysis of Spherical Data, Cambridge Press
 Gutiérrez, C.M., *et al.* 1999, astro-ph/9903196 (G99)
 Gutiérrez de la Cruz, C.M., *et al.* 1995, ApJ, 442, 10
 Haslam, C.G.T., *et al.* 1981, A&A, 100, 209
 Kogut, A., *et al.* 1996a, ApJ, 460, 1
 Kogut, A., *et al.* 1996b, ApJ, 464, L5
 Kogut, A. 1997, AJ, 114, 1127
 Kogut, A. 1999, in Microwave Foregrounds, ed. A. de Oliveira-Costa, and M. Tegmark (ASP, San Francisco), in press
 Leitch, E.M., *et al.* 1997, ApJ, 486, L23
 Lim, M.A., *et al.* 1996, ApJ, 469, L69

McCullough, P.R. 1997, AJ, 113, 2186
Platania, P., *et al.* 1998, ApJ, 505, 473
Reich, P., and Reich, W. 1988, A&AS, 74, 7

Rybicki, G. B. and Lightman, A. P. 1979, Radiative Processes
in Astrophysics, Wiley & Sons, p.174
Tegmark, M., *et al.* 1999, ApJ, in press